Available online at www.sciencedirect.com
ScienceDirect
Trans. Nonferrous Met. Soc. China 23(2013) 3677−3684
Transactions of Nonferrous Metals Society of China
www.tnmsc.cn

Microstructure and hydrogenation kinetics of Mg_2Ni-based alloys with addition of Nd, Zn and Ti

Wen-jie SONG, Jin-shan LI, Tie-bang ZHANG, Xiao-jiang HOU, Hong-chao KOU, Xiang-yi XUE, Rui HU

State Key Laboratory of Solidification Processing, Northwestern Polytechnical University, Xi'an 710072, China

Received 29 September 2012; accepted 15 January 2013

Abstract: In order to enhance the hydrogen absorption kinetics of the Mg_2Ni-based alloys, metal elements (Nd, Zn, and Ti) were added during melting process, respectively. The Mg_2Ni-based alloys were melted using an electric resistance furnace under the protection of the covering reagent to prevent the oxidation and the evaporation of magnesium. Phase compositions and microstructures of as-cast alloys were characterized by XRD and SEM equipped with EDS. Hydrogenation kinetics of experimental alloys were investigated by the constant volume method using a Sievert-type apparatus. The addition of Nd, Zn or Ti elements to Mg_2Ni results in the formation of minor phases Mg_6Ni and Ni_3Ti. Nd and Zn are dissolved in α-Mg, Mg_2Ni and $MgNi_2$ phases in Mg_2Ni-based alloys. With the addition of Nd, the hydrogen content of the first absorption is 2.86% in mass fraction, which is higher than that of the Mg_2Ni. Hydrogen absorption kinetics and activation properties of Mg_2Ni-based alloys are improved evidently. During the initial three hydrogenation/dehydrogenation cycles, the hydrogen absorption capacity and kinetics properties have been improved for alloys with the addition of transition element Zn or Ti. The kinetics properties of the experimental alloys and absorbing reaction mechanism were also analyzed with the help of the Hirooka kinetics model.
Key words: Mg_2Ni; hydrogen storage; kinetics; microstructure

1 Introduction

With the growing concern about environmental protection and shortage of the traditional energy, much attention has been paid to seeking clean energy sources during the past decades [1]. Hydrogen is considered an ideal medium of storage, transport and conversion of energy. Mg-based metal hydrides have been expected to be used as hydrogen storage materials because of their remarkable advantages, such as low specific mass, low cost and high hydrogen capacity, e.g. 7.6% (mass fraction) for MgH_2, 3.6% (mass fraction) for Mg_2NiH_4 [1,2]. However, the poor hydriding/dehydriding kinetics properties and their high corresponding temperatures make them far away from practical applications yet [3].

Many efforts have been paid to enhancing hydrogen absorption and desorption kinetics. Recently, many studies have been focused on improving the hydrogen storage performance of Mg_2Ni-type alloys by melt-spinning [4−7] and additives including transition metals [8−11], transition metal oxides [12,13] and carbon materials [14−16]. Nanocrystallization, amorphization and addition of transition metal elements have been demonstrated to improve the hydrogen absorption kinetics of Mg. By adding transition metals, such as Nb, Ti [17], V [8], Co [18], intermetallics with Ni are formed during solidification, and strongly catalyze the hydrogen absorption/desorption kinetics. Nb-based additives show excellent improvements in hydrogen sorption kinetics; Nb acts as a "gateway" for the hydrogen flowing in and out by forming niobium hydride (NbH_{1-x}) during the hydrogen sorption cycle [19,20]. The addition of rare earth elements, e.g. La, Y, Nd [21−23], makes alloys exhibit a higher hydrogen storage capacity. XIE et al [23] found that the $Mg_{1.9}Nd_{0.1}Ni$ alloy shows the best hydrogen absorption and desorption kinetics, the highest hydrogen capacity and good reversibility among $Mg_{2-x}Nd_xNi$ alloys. SPASSOV and STER [24] showed that rare earth Y or YNi_3 phase acts as an active site for hydriding/dehydriding, as well as it increases the lattice parameter of the alloy, which should lead to faster H-diffusion.

Transition metals and rare earth elements have been

Foundation item: Project (CX201107) supported by Doctorate Foundation of Northwestern Polytechnical University, China; Project (B08040) supported by the Program of Introducing Talents of Discipline to Universities ("111" Project), China
Corresponding author: Tie-bang ZHANG; Tel: +86-29-88491764; Fax: +86-29-88460294; E-mail: tiebangzhang@nwpu.edu.cn
DOI: 10.1016/S1003-6326(13)62916-7

reported possessing beneficial effect on the hydrogen absorption property, but which element has the better effect and the corresponding reaction mechanism is not clear. In this work, three elements are selected to add into Mg_2Ni alloy, respectively. They are f block rare earth element Nd, d block transition metal element Ti and ds block transition metal element Zn in periodic table. They substitute for Mg or Ni in Mg_2Ni alloy, respectively. In order to avoid the oxidation and evaporation of Mg, all alloys in this work are melted in an electrical resistance furnace under the protection of the cover reagent. The effects of Nd, Zn and Ti on phase composition, microstructure of Mg_2Ni-based alloys are investigated. The hydrogen absorbing kinetics properties of the experimental alloys and the reaction mechanism are analyzed with the help of the Hirooka kinetics model [25].

2 Experimental

Three kinds of Mg-based alloys with the composition of $Mg_{1.9}Nd_{0.1}Ni$, $Mg_2Ni_{0.9}Zn_{0.1}$ and $Mg_2Ni_{0.9}Ti_{0.1}$ were melted in the graphite crucible in an electric resistance furnace at 1023 K under the protection of the cover reagent. The cover reagent was prepared from $MgCl_2$, KCl, $BaCl_2$ and CaF_2. Commercially pure magnesium ingot (purity 99.9%), nickel powder (99.8%), neodymium powder (99.9%), zinc particles (99.9%) and titanium powder (99.9%) were used as raw materials. Due to the large difference of Mg and Ni in the melting temperatures and the high vapor pressure of melting Mg, the evaporation of Mg is serious, which results in the loss of Mg and the change of composition [24]. Considering the inherent evaporation of Mg and Nd elements during melting, the estimated losses for Mg and Nd were about 5% and 2%, respectively. Melting process was divided into two steps. Ni and transition metals were added after magnesium completely melted. In order to make all the metals fully melt and homogeneously mix, melting alloys were kept at 1023 K for 60 min and mechanically stirred frequently. The as-cast alloys were finally obtained after the melted alloys were taken out of the graphite crucible when they cooled down to room temperature.

The phase compositions and structures of the as-cast alloys were determined by an X-ray diffractometer (DX−2007) with Cu K_α radiation. The X-ray intensity was measured over a diffraction angle (2θ) 15°−80° with a velocity of 1.8 (°)/min, 35 kV and 35 mA. A scanning electron microscope (SEM) equipped with an energy dispersive X-ray spectrometer (EDS) was employed to characterize the microstructures, chemical composition, morphology and distribution of constituent phases.

The hydrogen absorption curves of the as-cast alloys were measured using an automatically controlled Sieverts apparatus. The hydrogen absorption was conducted at a hydrogen pressure of 4 MPa and 573 K.

3 Results and discussion

3.1 Phase composition analysis

Figure 1 shows the XRD patterns of the as-cast Mg_2Ni, $Mg_{1.9}Nd_{0.1}Ni$, $Mg_2Ni_{0.9}Ti_{0.1}$ and $Mg_2Ni_{0.9}Zn_{0.1}$ alloys. It can be seen that the major phase is Mg_2Ni in the as-cast Mg_2Ni alloy, and a little bit of Mg and $MgNi_2$ are included. With the addition of rare earth Nd, α-Mg phase disappeared, a minor phase was analyzed as Mg_6Ni except the major phase Mg_2Ni in $Mg_{1.9}Nd_{0.1}Ni$ alloy. The formation of Mg_6Ni phase is attributed to the solute accumulation in solidification. Minor impurity $MgCl_2$, which is residue of cover reagent, is found in $Mg_{1.9}Nd_{0.1}Ni$ alloy. With the addition of transition metal Zn, no difference is found in the phase constitution between Mg_2Ni and $Mg_2Ni_{0.9}Zn_{0.1}$ compared with as-cast Mg_2Ni alloy. The main difference is the intensity of the phases. The decrease of α-Mg intensity in $Mg_2Ni_{0.9}Zn_{0.1}$ reveals that α-Mg content is reduced. In addition, the $MgNi_2$ peak around 43.8° offsets to the low Bragg angle. The replacement of Zn to Ni in $MgNi_2$ results in the expansion of lattice. With the addition of transition metal Ti, the major phase is Mg_2Ni, and α-Mg phase increases obviously compared with Mg_2Ni alloy. Minor phase is included in $Mg_2Ni_{0.9}Ti_{0.1}$ alloy.

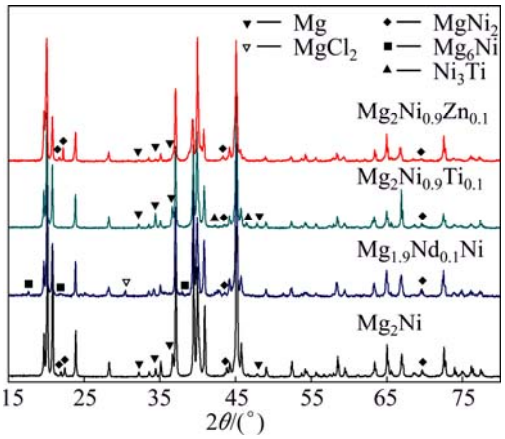

Fig. 1 XRD patterns of as-cast Mg_2Ni, $Mg_{1.9}Nd_{0.1}Ni$, $Mg_2Ni_{0.9}Zn_{0.1}$ and $Mg_2Ni_{0.9}Ti_{0.1}$ alloys

3.2 Microstructure, morphology and distribution of constituent phases

Figure 2 shows the SEM images of as-cast Mg_2Ni-based alloys. Table 1 gives the results of EDS analysis of the as-cast Mg_2Ni-based alloys. It is found that transition elements and rare earth elements reveal significant effects on microstructure, morphology and

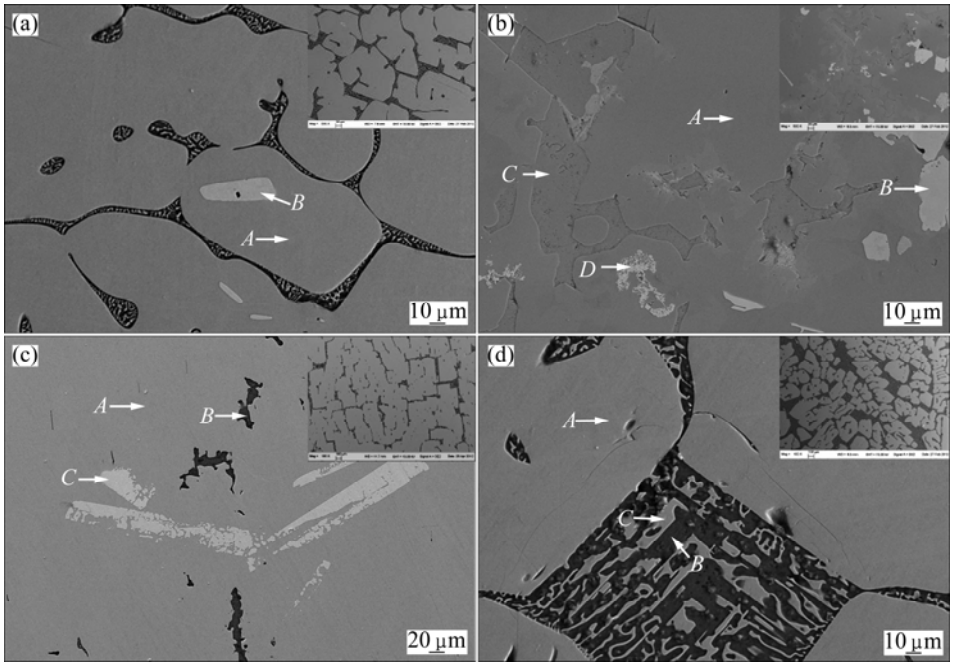

Fig. 2 SEM images of as-cast alloys: (a) Mg_2Ni; (b) $Mg_{1.9}Nd_{0.1}Ni$; (c) $Mg_2Ni_{0.9}Zn_{0.1}$; (d) $Mg_2Ni_{0.9}Ti_{0.1}$

Table 1 EDS analysis results in Fig. 2 for as-cast alloys

Alloy	Point	x(Mg)/%	x(Ni)/%	x(Nd)/%	x(Zn)/%	x(Ti)/%
Mg_2Ni	*A*	68.00	32.00	−	−	−
	B	37.46	62.54	−	−	−
$Mg_{1.9}Nd_{0.1}Ni$	*A*	67.68	31.51	0.81	−	−
	B	26.33	63.50	10.17	−	−
	C	88.17	5.93	5.90	−	−
	D	26.85	10.40	62.75	−	−
$Mg_2Ni_{0.9}Zn_{0.1}$	*A*	67.33	31.10	−	1.57	−
	B	98.81	0.48	−	0.71	−
	C	35.33	55.38	−	9.29	−
$Mg_2Ni_{0.9}Ti_{0.1}$	*A*	68.65	31.35	−	−	0
	B	99.35	0.65	−	−	0
	C	68.44	31.56	−	−	0

distribution of constituent phases. The insert images in the top right corner of the four micrographs are the corresponding low power micrographs. There are three phases including Mg_2Ni, α-Mg and $MgNi_2$ in the as-cast Mg_2Ni alloy. The main phase is Mg_2Ni, the eutectic structure of Mg and Mg_2Ni is in the interphase area of Mg_2Ni phase. The small white polygons embedded in the Mg_2Ni are identified as $MgNi_2$ phase, which is primary $MgNi_2$ phase. During the solidification process of the Mg_2Ni alloy, the $MgNi_2$ phase precipitates from the liquid phase with the temperature decreasing. Then the peritectic product Mg_2Ni is formed with the reaction of $MgNi_2$ and liquid phase, but the peritectic reaction does not proceed completely, and remnant $MgNi_2$ phase retains inside Mg_2Ni phase. With the temperature decreasing, the eutectic reaction takes place and the eutectic structure including Mg and Mg_2Ni phases is formed.

There are at least four phases in $Mg_{1.9}Nd_{0.1}Ni$ alloy, including the solid solutions of Nd element in α-Mg, Mg_2Ni, $MgNi_2$ phases and Nd-rich phase. Mg_6Ni and $MgCl_2$ are not detected in the sample by SEM-EDS. The eutectic Mg and Mg_2Ni structure is not observed in $Mg_{1.9}Nd_{0.1}Ni$, as shown in Fig. 2(b). The content of $MgNi_2$ intermetallic compound in $Mg_{1.9}Nd_{0.1}Ni$ alloy is greater than that in Mg_2Ni alloys because the substitution of Mg by Nd in $Mg_{1.9}Nd_{0.1}Ni$ alloy results in the increase of mole ratio of Ni to Mg. The content of Nd in $MgNi_2$ is more than that in α-Mg or Mg_2Ni phase.

There are three phases in $Mg_2Ni_{0.9}Zn_{0.1}$ alloy, which are analyzed as the solid solution of Zn in Mg, Mg_2Ni and $MgNi_2$, respectively. Mg and Mg_2Ni eutectic

structure exists at the interface of Mg_2Ni phase.

Only two phases, α-Mg and Mg_2Ni, are found in $Mg_2Ni_{0.9}Ti_{0.1}$ alloy from the micrograph of Fig. 2(d). The α-Mg and Mg_2Ni eutectic structure in $Mg_2Ni_{0.9}Ti_{0.1}$ alloy significantly increases compared with Mg_2Ni alloy. Analysis from alloy phase diagrams of Mg−Ni shows that the increase of eutectic structure must result from the decrease of Ni content. With the decrease of Ni content, more Mg and Mg_2Ni eutectic structures are generated during the process of solidification. The decrease of Ni element in as-cast alloy may be explained by the reaction between Ni and Ti during the melting process and the serious composition segregation. The result of XRD shows only a little Ni_3Ti contained in alloy. The cast ingot of $Mg_2Ni_{0.9}Ti_{0.1}$ is separated into two layers obviously. The hardness of the low layer is larger than that of the top one, and the luster is different. Hence, the two layers are different alloys.

3.3 Hydrogen absorption kinetics

The first hydrogen absorption kinetics curves of the as-cast Mg_2Ni, $Mg_{1.9}Nd_{0.1}Ni$, $Mg_2Ni_{0.9}Ti_{0.1}$ and $Mg_2Ni_{0.9}Zn_{0.1}$ alloys at 573 K and 4 MPa are shown in Fig. 3. The initial hydrogen-absorbing capacities of all alloys in this work fail to meet the theoretical hydrogen absorption capacity. Due to the exposure of alloy powders to air, impurity gas in air has certain effect on alloy surfaces, impurity gas is adsorbed and passive film forms on the surface of alloy particles [26]. In order to absorb hydrogen effectively, fresh metallic surface must be exposed for the dissociation of hydrogen, allowing the subsequent absorption of atomic hydrogen [26]. Another reason for failing to meet theoretical capacity is that the kinetics curves are the results of the first hydrogen absorbing measurement, and alloys have not been activated completely. From these curves, it can be obtained that with the addition of transition metal

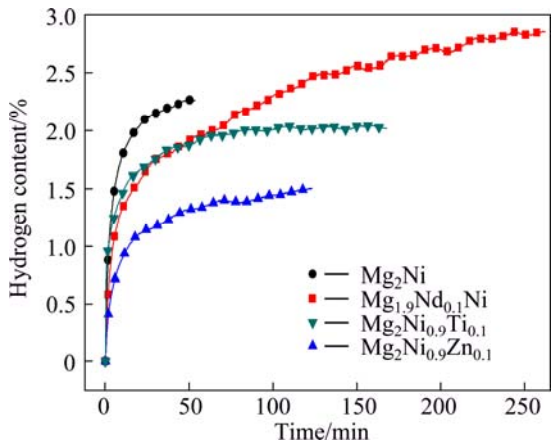

Fig. 3 Initial hydrogen absorption curves of as-cast Mg_2Ni, $Mg_{1.9}Nd_{0.1}Ni$, $Mg_2Ni_{0.9}Ti_{0.1}$ and $Mg_2Ni_{0.9}Zn_{0.1}$ alloys at 573 K and 4 MPa

elements, the content of the first absorbed hydrogen of as-cast $Mg_2Ni_{0.9}Zn_{0.1}$ and $Mg_2Ni_{0.9}Ti_{0.1}$ alloys is lower than that of as-cast Mg_2Ni in initial 60 min, and the kinetics property is lower than that of as-cast Mg_2Ni. With the addition of Nd, the amount of the first absorbed hydrogen is 2.86% in mass fraction, which is higher than that of as-cast Mg_2Ni. The substitution of Nd for Mg has improved the activation property of Mg_2Ni alloy.

Figure 4 shows hydrogen absorption curves of the as-cast Mg_2Ni, $Mg_{1.9}Nd_{0.1}Ni$, $Mg_2Ni_{0.9}Zn_{0.1}$ and $Mg_2Ni_{0.9}Ti_{0.1}$ alloys. Figure 4(a) depicts that the amount of absorbed hydrogen of Mg_2Ni is 2.27% (mass fraction) and hydrogen absorption reaches equilibrium within 60 min. The substitution of Nd for Mg has improved the activation properties of Mg_2Ni alloy [23]. $Mg_{1.9}Nd_{0.1}Ni$ alloy can be activated after only one hydrogen absorption–desorption cycle under a hydrogen pressure of 4 MPa at 573 K. Insert figure in Fig. 4(b) shows the initial three hydrogen absorption and desorption cycles of $Mg_{1.9}Nd_{0.1}Ni$ at 573 K and 623 K. With the addition of Nd, the amount of the first hydrogen absorption achieves 2.86% in mass fraction, higher than that of Mg_2Ni. The amount of the second hydrogen absorption is 2.72% in mass fraction, and $Mg_{1.9}Nd_{0.1}Ni$ alloy can absorb 80% of the hydrogen absorption capacity within 144 s. Thus, it is believed that $Mg_{1.9}Nd_{0.1}Ni$ alloy has been activated. In the third cycle, hydrogen absorption reaches the saturated hydrogen capacity within 500 s. Compared the second saturated hydrogen capacity with the third one, the curves indicate that the saturated hydrogen capacity at 623 K is lower than that at 573 K. With the increase of temperature, more and more hydrogen is desorbed during the hydrogen absorption processes [27]. Thus, the hydrogen absorption capacity at higher temperature is lower than that at lower temperature.

The substitution of Zn for Ni has decreased the hydrogen absorption capacity and kinetics of Mg_2Ni alloy, which can be seen in Fig. 4(c). The hydrogen absorption capacity and kinetics increase with the increasing cyclic time. With the addition of Ti to Mg_2Ni alloy, the hydrogen absorption capacity increases with the increasing cyclic time, as shown in Fig. 4(d). The increasing cycle is beneficial to the activation of alloy, which further promotes the absorbing capacity and kinetics.

The hydrogen absorbing reaction mechanism is proposed by comparing the observed absorption rate with Hirooka kinetics model [25]. The hydrogen absorbing reaction rate to reach equilibrium is proportional to the deviation from the equilibrium. The reaction rate is controlled by the hydrogen diffusion in the metals. The model equation is as follows:

$$\ln[(p-p_f)/(p_i-p_f)] = -k_\alpha t \quad (1)$$

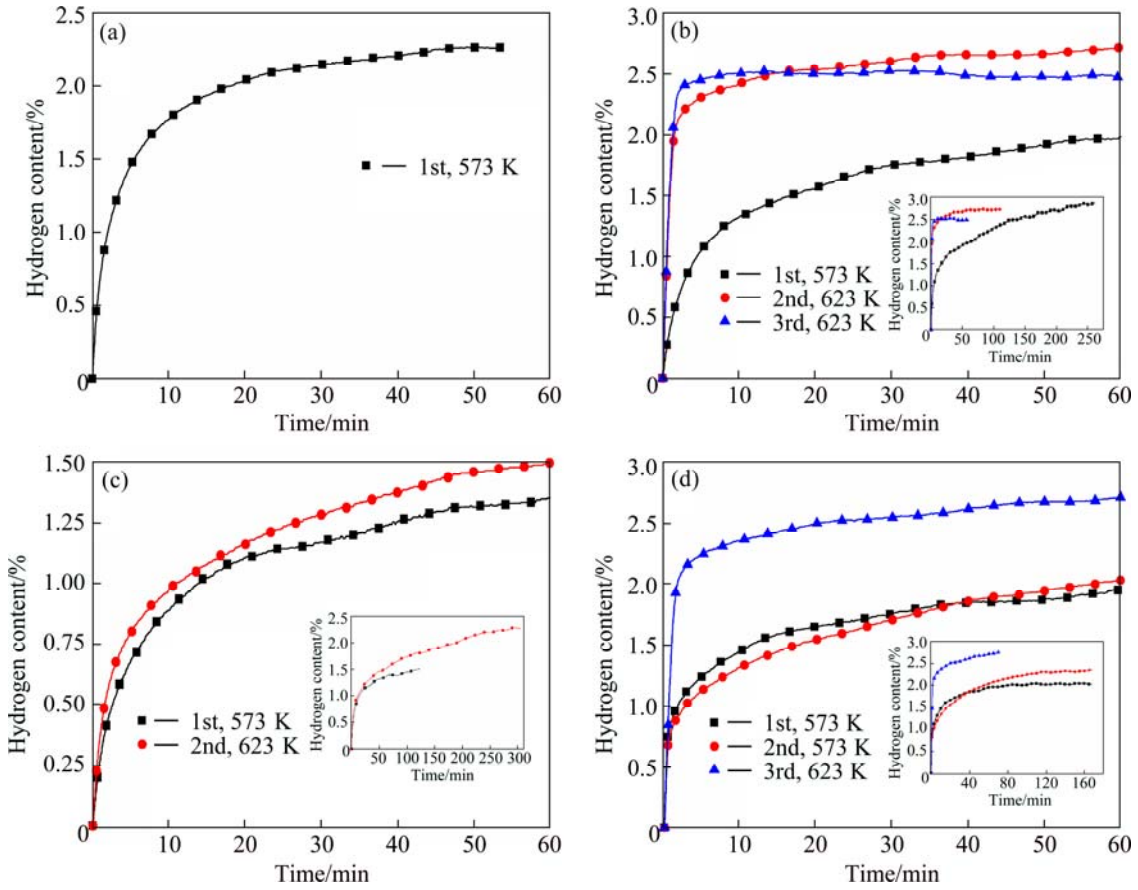

Fig. 4 Initial three hydrogen absorption curves of as-cast alloys within 60 min: (a) Mg_2Ni; (b) $Mg_{1.9}Nd_{0.1}Ni$; (c) $Mg_2Ni_{0.9}Zn_{0.1}$; (d) $Mg_2Ni_{0.9}Ti_{0.1}$ (Insert figures are initial hydrogen absorption curves reaching hydrogen absorbing equilibrium of Mg_2Ni-based alloys)

where k_α is defined as the absorption rate constant; p is hydrogen pressure; p_i is the initial hydrogen pressure; t is arbitrary time; p_f is the equilibrium hydrogen pressure.

The kinetics analyses of the initial hydrogen absorption behavior for Mg_2Ni-based alloys are shown in Fig. 5. It is easy to conclude that the hydrogenation process can be divided into the rapid absorbing stage (stage 1) and the stable absorbing one (stage 2) [28]. The corresponding slopes of the absorbing stage straight lines given by plotting the left-hand values of Eq. (1) against time are designed as $k_{\alpha 1}$ and $k_{\alpha 2}$, respectively [25]. The hydrogen absorption reaction rate constants calculated from the slopes are summarized in Table 2.

The reaction rate ($k_{\alpha 1}$) in the first stage is larger than that ($k_{\alpha 2}$) in the second stage, and the variation in the slopes indicates that the hydrogen absorption reaction mechanism changes during hydrogenation. Diffusion rate of hydrogen atom through the hydride phase is different from that through Mg. In the α phase region, hydrogen atoms diffuse into the interstitial site of metals and alloys lattice, forming solid solution α phase. In the (α+β) phase region, the hydrogen is able to penetrate through grain boundaries (interface) and to dissolve in the bulk. With the increase of hydrogen concentration, hydride nucleates on the particle surface and at grain boundaries (interface), and grain defect locations are always nucleation sites. Hydride grows and the continuous hydride layer is formed. On the contrary, in the β-phase region, hydrogen atoms get redistributing in the hydride phase diffusing towards the grain centers. Major differences between the two regions relevant to the hydrogen absorption mechanism are the different relative volume expansion associated with each of these transformations. With the increase of hydrogen concentration, the volume of the grain is expanded gradually. The large volume expansion causes the reacting grains to be pressed together. This applied pressure gradually narrows the channel of transfer, reducing the hydrogen flowing into the deeper parts of the sample [27,29]. Furthermore, diffusivity of hydrogen through the hydride phase is much smaller than that through Mg. As the continuous hydride layer is formed, the reaction rate slows down and the reaction moves into stage 2 ($k_{\alpha 2}$). The reaction rate of the second stage is restricted by the diffusion rate of hydrogen through hydride layer.

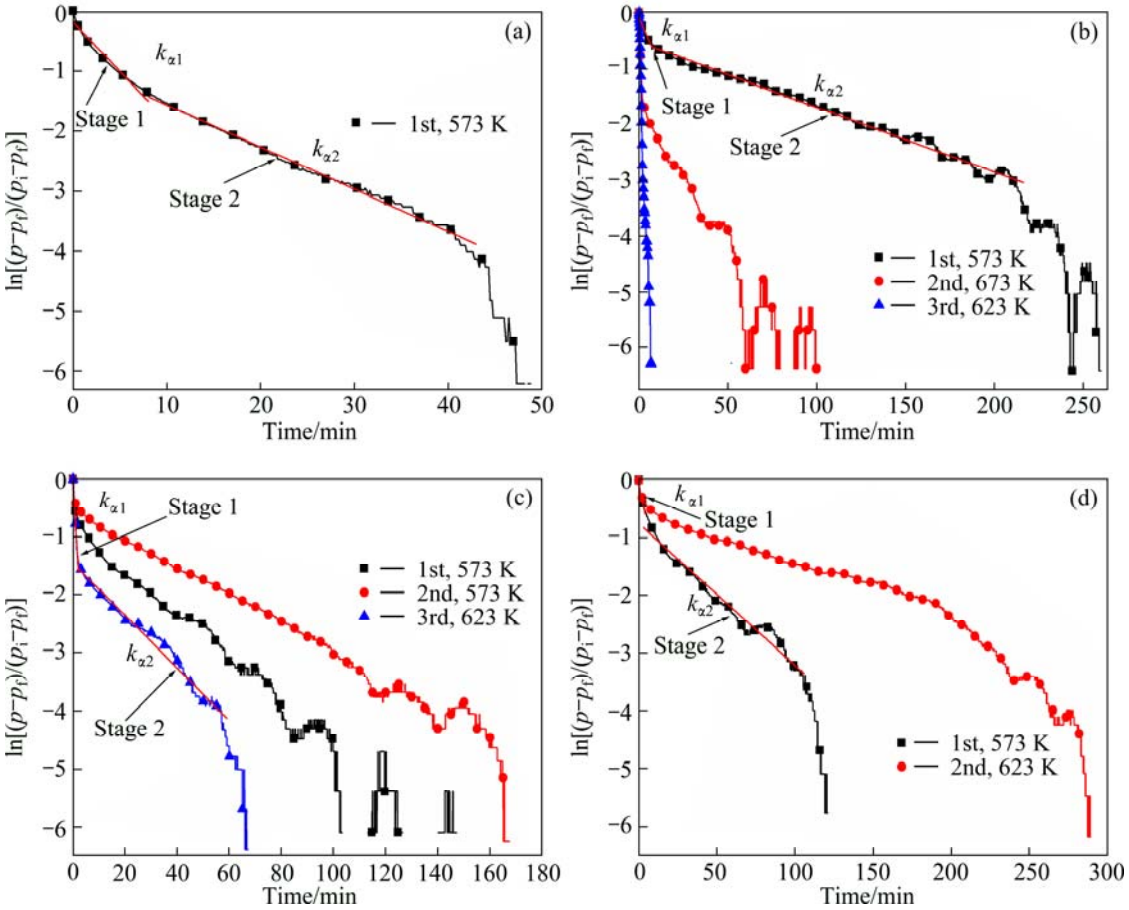

Fig. 5 Kinetics analyses of initial three hydrogen absorption behaviors: (a) Mg_2Ni; (b) $Mg_{1.9}Nd_{0.1}Ni$; (c) $Mg_2Ni_{0.9}Ti_{0.1}$; (d) $Mg_2Ni_{0.9}Zn_{0.1}$

Table 2 Hydrogen absorbing reaction rate constants of experimental Mg_2Ni-based alloys

Alloy	1st cycle		2nd cycle		3rd cycle	
	$k_{\alpha1}$	$k_{\alpha2}$	$k_{\alpha1}$	$k_{\alpha2}$	$k_{\alpha1}$	$k_{\alpha2}$
Mg_2Ni	0.20561	0.07107	–	–	–	–
$Mg_{1.9}Nd_{0.1}Ni$	0.05974	0.013	0.79202	0.0487	1.40602	0.5469
$Mg_2Ni_{0.9}Zn_{0.1}$	0.08251	0.02437	0.12121	0.02466	–	–
$Mg_2Ni_{0.9}Ti_{0.1}$	0.45958	0.03806	0.35056	0.02467	0.78003	0.04493

The amount of hydrogen absorption in rapid absorbing stage is related to the hydride nucleation rate. The magnesium hydride preferentially nucleates on the surface of metal particles and at grain boundary. As the coverage with hydride increases with time, less area for hydrogen atoms entry will be available, leading to a decrease in the growth rate and the hydrogen absorption rate. When the hydride colonies/crystals impinge on each other, the hydrogenation rate will be decreased significantly and a pseudo-saturation will be reached. This pseudo-saturation level is considered the hydrogen absorption capacity, which is defined as the hydrogen content after a long hydrogenation period at a given temperature and pressure [30]. Then the hydrogen absorption enters into the stable absorbing stage (stage 2). The increase of hydrogen absorption content is limited in this stage. When the hydride nucleation rate is high, the hydride colonies/crystals impinge on each other very quickly, and the continuous hydride layer is formed. So, the layer is very thin, and the amount of hydrogen absorption in rapid absorbing stage is low. On the contrary, the amount of hydrogen absorption increases when the hydride nucleation rate is reduced [30]. As shown in Fig. 4 and Fig. 5, the contents of hydrogen absorption and reaction rate in rapid absorbing stage increase with the increase of temperature. The enhancement of hydrogen capacity by increasing the hydrogenation temperature can be attributed to the

reduced nucleation rate [30].

The good activation property and hydrogen absorption kinetics of $Mg_{1.9}Nd_{0.1}Ni$ alloy are strongly dependent on the microstructure and phase constituent [3]. The multiphase structures involving Mg_2Ni, $MgNi_2$, α-Mg and Mg_6Ni increase the interface area that provides favorable diffusion channels for hydrogen atoms and buffer area for the release of the distortion and stress of the crystal lattice. Some alloy particles existing in the hydride layer can provide diffusion pathways for hydrogen atoms, thereby reduce the reaction activation energy and improve the hydrogen absorption rates [23]. The atomic radius of Nd is larger than that of Mg or Ni, so the substitution of Nd for Mg or Ni leads to the expansion of lattice of Mg−Ni alloy. It is beneficial for hydrogen atoms to diffuse through hydride layer. Furthermore, the hydrogen absorption and desorption processes cause expansion and contraction of the crystal lattice which induces many defects inevitably. These defects can serve as preferable nucleation sites for MgH_2 and Mg_2NiH_4 formation [23]. However, the hydrogen storage content decreases with the cyclic time. It also can be seen in the work of XIE et al [23]. Nd hydride has catalytic effect on hydrogen absorption process, but it is thermally stable [23], so it is hard to dehydrogenate. With the addition of Ti or Zn, the amount of the first hydrogen absorption is lower than that of the Mg_2Ni alloy, and the hydrogen absorption capacity increases with the increasing cyclic time in the first three hydrogen absorbing processes. $MgNi_2$ cannot be hydrogenated, the substitution of Zn to Ni in $MgNi_2$ phase suppresses the formation of hydride and reduces the area of hydrogen atom diffusion. Thus, the $Mg_2Ni_{0.9}Zn_{0.1}$ alloy reveals low hydrogen absorption content and slow hydrogen absorption kinetics. With the addition of Ti, the Mg phase increases, so the hydrogen absorption capacity of $Mg_2Ni_{0.9}Ti_{0.1}$ alloy increases. The absorption capacity increases with the increasing cycle time due to the growing number of grain defects and diffusion channel. The initial three hydrogen absorption capacities of $Mg_2Ni_{0.9}Ti_{0.1}$ alloy are 2.0%, 2.35% and 2.76% in mass fraction, respectively. The content of the third hydrogen absorption is higher than that of the $Mg_{1.9}Nd_{0.1}Ni$ alloy.

4 Conclusions

1) The addition of Nd, Ti or Zn element results in the formation of minor phases Mg_6Ni and Ni_3Ti. Nd and Zn are dissolved in α-Mg, Mg_2Ni and $MgNi_2$ phases in Mg_2Ni-based alloys.

2) The as-cast Mg_2Ni alloy contains Mg_2Ni, $MgNi_2$, Mg and Mg_2Ni eutectic structure. The addition of Nd results in the disappearance of eutectic structure of Mg and Mg_2Ni. Nd is dissolved into α-Mg, Mg_2Ni and $MgNi_2$ phases. The content of $MgNi_2$ intermetallic compound is higher than that in Mg_2Ni alloys. Zn is dissolved into α-Mg, Mg_2Ni and $MgNi_2$ phases in $Mg_2Ni_{0.9}Zn_{0.1}$ alloy. $MgNi_2$ intermetallic compound appears block or plate strip. With the addition of Ti element, $MgNi_2$ disappears and eutectic structure of Mg and Mg_2Ni increases compared with Mg_2Ni alloy.

3) With the addition of Nd, the hydrogen content of the first absorption of $Mg_{1.9}Nd_{0.1}Ni$ is 2.86% in mass fraction, which is higher than that of as-cast Mg_2Ni. With the addition of transition metal element, the amount of first absorbed hydrogen and kinetics of as-cast $Mg_2Ni_{0.9}Zn_{0.1}$ and $Mg_2Ni_{0.9}Ti_{0.1}$ alloys are lower compared with as-cast Mg_2Ni in initial 60 min. During the initial three hydrogenation/dehydrogenation cycles, the hydrogen absorption capacity and kinetics properties of Mg_2Ni have been improved with the addition of transition element Zn or Ti. The $Mg_{1.9}Nd_{0.1}Ni$ preserves better activation properties compared with the Zn- or Ti-doped Mg_2Ni alloy.

4) The capacity of hydrogen absorption in rapid absorbing stage is related to the hydride nucleation rate, which is related to the temperature and the particle surface phase. Hydrogenation/dehydrogenation cycle increases defect and diffusion channel, which is beneficial to increasing nucleation site near surface and enlarge diffusion area of hydrogen atom in rapid absorbing stage.

References

[1] JAIN I P, LAL C, JAIN A. Hydrogen storage in Mg: A most promising material [J]. Int J Hydrogen Energy, 2010, 35(10): 5133−5144.

[2] SCHLAPBACH L, ZÜTTEL A. Hydrogen-storage materials for mobile applications [J]. Nature, 2001, 414(6861): 353−358.

[3] YIM C D, YOU B S, NA Y S, BAE J S. Hydriding properties of Mg−xNi alloys with different microstructures [J]. Catal Today, 2007, 120(3−4): 276−280.

[4] ZHANG Y H, ZHAO D L, LI B W, QI Y, GUO S H, WANG X L. Hydrogen storage behaviours of nanocrystalline and amorphous $Mg_{20}Ni_{10-x}Co_x$(x=0−4) alloys prepared by melt spinning [J]. Transactions of Nonferrous Metals Society of China, 2010, 20(3): 405−411.

[5] ZHANG Y H, LI B W, REN H P, GUO S H, ZHAO D L, WANG X L. Hydrogenation and dehydrogenation behaviours of nanocrystalline $Mg_{20}Ni_{10-x}Cu_x$ (x=0−4) alloys prepared by melt spinning [J]. Int J Hydrogen Energy, 2010, 35(5): 2040−2047.

[6] KALINICHENKA S, RÖNTZSCH L, RIEDL T, GEMMING T, WEIBGÄRBER T, KIEBACK B. Microstructure and hydrogen storage properties of melt-spun Mg−Cu−Ni−Y alloys [J]. Int J Hydrogen Energy, 2011, 36(2): 1592−1600.

[7] ZHANG Y H, LÜ K, ZHAO D L, GUO S H, QI Y, WANG X L. Electrochemical hydrogen storage characteristics of nanocrystalline and amorphous Mg_2Ni-type alloys prepared by melt-spinning [J]. Transactions of Nonferrous Metals Society of China, 2011, 21(3): 502−511.

[8] CHO Y H, AMINORROAYA S, LIU H K, DAHLE A K. The effect

of transition metals on hydrogen migration and catalysis in cast Mg−Ni alloys [J]. Int J Hydrogen Energy, 2011, 36(8): 4984−4992.

[9] AMINORROAYA S, RANJBAR A, CHO Y H, LIU H K, DAHLE A K. Hydrogen storage properties of Mg−10 wt% Ni alloy co-catalysed with niobium and multi-walled carbon nanotubes [J]. Int J Hydrogen Energy, 2011, 36(1): 571−579.

[10] ZHANG Y H, ZHAO D L, LI B W, REN H P, GUO S H, WANG X L. Electrochemical hydrogen storage characteristics of nanocrystalline $Mg_{20}Ni_{10-x}Cu_x$ (x=0−4) alloys prepared by melt-spinning [J]. J Alloys Compd, 2010, 491(1−2): 589−594.

[11] HUANG L W, ELKEDIM O, JARZEBSKI M, HAMZAOUI R, JURCZYK M. Structural characterization and electrochemical hydrogen storage properties of $Mg_2Ni_{1-x}Mn_x$(x=0, 0.125, 0.25, 0.375) alloys prepared by mechanical alloying [J]. Int J Hydrogen Energy, 2010, 35(13): 6794−6803.

[12] AGUEY-ZINSOU K F, ARES FERNANDEZ J R, KLASSEN T, BORMANN R. Effect of Nb_2O_5 on MgH_2 properties during mechanical milling [J]. Int J Hydrogen Energy, 2007, 32(13): 2400−2407.

[13] OELERICH W, KLASSEN T, BORMANN R. Metal oxides as catalysts for improved hydrogen sorption in nanocrystalline Mg-based materials [J]. J Alloys Compd, 2001, 315(1−2): 237−242.

[14] MILANESE C, GIRELLA A, GARRONI S, BRUNI G, BERBENNI V, MATTEAZZI P, MARINI A. Effect of C (graphite) doping on the H_2 sorption performance of the Mg−Ni storage system [J]. Int J Hydrogen Energy, 2010, 35(3): 1285−1295.

[15] SINGH R K, RAGHUBANSHI H, PANDEY S K, SRIVASTAVA O N. Effect of admixing different carbon structural variants on the decomposition and hydrogen sorption kinetics of magnesium hydride [J]. Int J Hydrogen Energy, 2010, 35(9): 4131−4137.

[16] AMINORROAYA S, LIU H K, CHO Y, DAHLE A. Microstructure and activation characteristics of Mg−Ni alloy modified by multi-walled carbon nanotubes [J]. Int J Hydrogen Energy, 2010, 35(9): 4144−4153.

[17] PHETSINORATH S, ZOU J X, ZENG X Q, SUN H Q, DING W J. Preparation and hydrogen storage properties of ultrafine pure Mg and Mg–Ti particles [J]. Transactions of Nonferrous Metals Society of China, 2012, 22(8): 1849−1854.

[18] ZHANG Y H, SONG C H, REN H P, LI Z G, HU F, ZHAO D L. Enhanced hydrogen storage kinetics of nanocrystalline and amorphous Mg_2Ni-type alloy by substituting Ni with Co [J]. Transactions of Nonferrous Metals Society of China, 2011, 21(9): 2002−2009.

[19] PELLETIER J F, HUOT J, SUTTON M, SCHULZ R, SANDY A R, LURIO L B, MOCHRIE S G J. Hydrogen desorption mechanism in MgH_2−Nb nanocomposites [J]. Phys Rev B, 2001, 63(5): 052103.

[20] KIM J W, AHN J P, KIM D H, CHUNG H S, SHIM J H, CHO Y W, OH K H. In situ transmission electron microscopy study on microstructural changes in NbF_5-doped MgH_2 during dehydrogenation [J]. Scr Mater, 2010, 62(9): 701−704.

[21] KAZUHIDE T. Hydride stability and hydrogen desorption characteristics in melt-spun and nanocrystallized Mg–Ni–La alloy [J]. J Alloys Compd, 2008, 450(1−2): 432−439.

[22] KALINICHENKA S, RONTZSCH L, RIEDL T, WEIBGÄRBER T, KIEBACK B. Hydrogen storage properties and microstructure of melt-spun $Mg_{90}Ni_8RE_2$ (RE=Y, Nd, Gd) [J]. Int J Hydrogen Energy, 2011, 36(17): 10808−10815.

[23] XIE D H, LI P, ZENG C X, SUN J W, QU X H. Effect of substitution of Nd for Mg on the hydrogen storage properties of Mg_2Ni alloy [J]. J Alloys Compd, 2009, 478(1−2): 96−102.

[24] SPASSOV T, KÖSTER U. Thermal stability and hydriding properties of nanocrystalline melt-spun $Mg_{63}Ni_{30}Y_7$ alloy [J]. J Alloys Compd, 1998, 279(2): 279−286.

[25] HIROOKA Y, MIYAKE M, SANO T. A study of hydrogen absorption and desorption by titanium [J]. J Nucl Mater, 1981, 96(3): 227−232.

[26] BROOM D P. Hydrogen storage materials: The characterisation of their storage properties [M]. London: Springer-Verlag; 2011.

[27] YANG X W, ZHANG T B, HU R, LI J S, XUE X Y, FU H Z. Microstructure and hydrogenation thermokinetics of ZrTi0.2V1.8 alloy [J]. Int J Hydrogen Energy, 2010, 35(21): 11981−11985.

[28] ZHANG T B, WANG X F, HU R, LI J S, YANG X W, XUE X Y, FU H Z. Hydrogen absorption properties of $Zr(V_{1-x}Fe_x)_2$ intermetallic compounds [J]. Int J Hydrogen Energy, 2012, 37(3): 2328−2335.

[29] BLOCH J. The temperature-dependent changes of the kinetics and morphology of hydride formation in zirconium [J]. J Alloys Compd, 1995, 216(2): 187−195.

[30] TIEN H Y, TANNIRU M, WU C Y, EBRAHIMI F. Mechanism of hydrogen capacity dependence on the hydrogenation temperature [J]. Scr Mater, 2010, 62(5): 274−277.

添加 Nd、Zn、Ti 的 Mg_2Ni 基合金微观组织及氢化动力学

宋文杰，李金山，张铁邦，侯小江，寇宏超，薛祥义，胡 锐

西北工业大学 凝固技术国家重点实验室，西安 710072

摘 要：为了提高 Mg_2Ni 基合金的储氢动力学性能，通过熔炼方法分别添加金属元素 Nd，Zn 和 Ti 来防止镁的氧化和蒸发，将 Mg_2Ni 基合金在有覆盖剂保护的电阻炉中进行熔炼。借助 XRD 和 SEM/EDS 研究了铸态合金的相组成和微观组织。采用定容法在 Sievert's 型 PCT 测试仪上测试了合金的氢化动力学性能。Nd、Zn 和 Ti 的添加导致了微量相 Mg_6Ni 和 Ni_3Ti 的生成。Nd 和 Zn 溶解在 Mg_2Ni 基合金的 α-Mg、Mg_2Ni 和 $MgNi_2$ 相中。添加 Nd 元素后，合金的首次吸氢量高于 Mg_2Ni 的，达到 2.86%(质量分数)。Mg_2Ni 基合金的吸氢动力学性能和活化性能均有所提高。在前 3 次吸放氢循环过程中，添加 Zn 和 Ti 的合金吸氢量和吸氢动力学性能均得到提高。采用 Hirooka 动力学模型分析了合金的氢化动力学性能及反应机制。

关键词：Mg_2Ni；储氢；动力学；微观组织

(Edited by Hua YANG)